International Journal of Fluid Mechanics Research, Vol. 31, No. 3, 2004

Natural Convection of Liquid Metals in an Inclined Enclosure in the Presence of a Magnetic Field[†]

Ali Al-Mudhaf and **Ali J. Chamkha**
Manufacturing Engineering Department
The Public Authority for Applied Education and Training
P. O. Box 42325, Shuweikh, 70654 Kuwait

The problem of steady, laminar, natural convective flow of electrically-conducting liquid metals such as gallium and germanium in an inclined rectangular enclosure in the presence of a uniform magnetic field is considered. Transverse gradient of heat is applied on two opposing walls of the inclined enclosure while the other two walls are adiabatic. A magnetic field is applied normal to the non-insulated walls. The problem is formulated in terms of the vorticity – stream function procedure. A numerical solution based on the finite-difference method is obtained. Representative results illustrating the effects of the enclosure inclination angle and the Hartmann number for two different Rayleigh numbers on the contour maps of the streamlines and temperature as well as the profiles of velocity components and temperature at mid-section of the enclosure are reported. In addition, results for the average Nusselt number are presented and discussed for various parametric conditions.

* * *

Nomenclature

b	inertia coefficient of porous medium;
A	enclosure aspect ratio, H/W;
B_0	magnetic induction;
g	gravitational acceleration;
H	enclosure height;
Ha	Hartmann number, $B_0 W\sqrt{\sigma/\rho\nu}$;
$\overline{\mathrm{Nu}}$	average Nusselt number at heated vertical wall;
p	fluid pressure;
Pr	Prandtl number, ν/α_t;
Ra	thermal Rayleigh number, $\mathrm{g}\beta_T(T_h - T_c)W^3/(\alpha_t\nu)$;
t	time;

[†]Received 17.05.2004

ISSN 1064-2277

T temperature;
T_h hot wall temperature (source);
T_c cold wall temperature (sink);
u x-component of velocity;
U dimensionless X-component of velocity, uW/α_t;
v y-component of velocity;
V dimensionless Y-component of velocity, vW/α_t;
W enclosure width;
x distance along insulated walls;
X dimensionless distance along insulated walls, x/W;
y distance normal to insulated walls;
Y dimensionless distance normal to insulated walls, y/W.

Greek Symbols

α enclosure inclination angle;
α_t thermal diffusivity;
β_T thermal expansion coefficient;
ν kinematic viscosity;
θ dimensionless temperature, $(T - T_c)/(T_h - T_c) - 0.5$;
ρ density;
σ electrical conductivity;
τ dimensionless time, $\alpha_t t/W^2$;
Ω vorticity;
ψ dimensionless stream function, Ψ/α_t;
Ψ stream function;
ζ dimensionless vorticity, $\Omega W^2/\alpha_t$;
∇^2 Laplacian operator.

Introduction

In recent years, various studies dealing with natural convection in inclined enclosures have been reported. These studies show that tilting the enclosure have significant effect on the flow and heat transfer characteristics. For instance, in crystal growth processes from melts, it has been reported by Markham and Rosenberger [1] that larger transport rated are obtained by tilting the ampoule. Motivated by this, Bontoux et al. [2] have carried out a numerical and experimental investigation on three-dimensional buoyancy-driven flows in a tilted cylinder (ampoule) with axial heating. Many other examples on the effect of inclination on natural convection flows have been reported by Delgado-Buscalioni and Crespo del Arco [3]. For example, it has been proven that significant heat transfer enhancement can be obtained when the tube in a heat exchanger is optimally inclined (see Lock and Fu [4]). Other applications of inclined configurations are the honeycomb solar collector plates [5, 6], spread of radioactive materials in long tilted liquid-filled rock fractures [7] and geophysical situations where a fluid is enclosed in narrow slots arbitrarily inclined to gravity [7, 8]. Also, Cerisier and Rahal [9] have employed inclined geometries in their experimental investigation on natural convection in enclosures with axial and lateral heating to study the interaction between longitudinal and transversal instabilities.

Natural convection in enclosures in the presence of magnetic fields has also received considerable attention in recent years due to possible applications in many industrial and technological fields

such as fusion reactors [10] and crystal growth [11]. For example, Oreper and Szekely [11] have found that the strength of the magnetic field is one of the important factors in determining the quality of the crystal. This is related to the fact that during a crystal growth process, some turbulence in the natural convection currents occurs. This can be suppressed by the application of a magnetic field. Ozoe and Maruo [12] have investigated magnetic and gravitational natural convection of melted silicon-two dimensional numerical computations for the rate of heat transfer. Garandet et al. [13] and Alchaar et al. [14] have studied natural convection heat transfer in a rectangular enclosure with a transverse magnetic field. Buhler [15] has considered magnetohydrodynamic (MHD) flows in arbitrary geometries in strong magnetic fields related to the design of fusion reactor blankets. Viskanta et al. [16] have studied three-dimensional natural convection heat transfer of a liquid metal in a cavity. Tagawa and Ozoe [17, 18] have reported on the enhancement of heat transfer rate by the application of a static magnetic field in a cubical enclosure. Recently, Di Piazzo and Ciofalo [10, 19] have analyzed MHD free convection in a liquid-metal filled cubic enclosure for the conditions of differential heating [10] and internal heating [19]. The effect of a magnetic field on free convection in a rectangular enclosure has also been studied by Rudraiah et al. [20] and Al-Najem et al. [21].

The objective of this work is to consider laminar, two-dimensional natural convection flow due to a transverse temperature gradient inside an inclined rectangular enclosure filled with electrically-conducting liquid metals such as gallium and germanium in the presence of a uniform magnetic field. This work has direct applications in the field of crystal growth and semiconductor production.

1. Mathematical Model

Consider laminar, two-dimensional, hydromagnetic, natural convective flow of a liquid metal such as gallium and germanium inside an inclined rectangular enclosure in the presence of a uniform magnetic field. The temperatures T_h and T_c are uniformly imposed on two opposing walls such that $T_h > T_c$ while the other two walls are assumed to be adiabatic. Fig. 1 shows the schematic of the problem under consideration. The fluid is assumed to be incompressible, Newtonian, viscous and electrically-conducting. The magnetic Reynolds number is assumed to be small so that the induced magnetic field is neglected. The small magnetic Reynolds number assumption is widely used and it uncouples Maxwell's equations from the Navier – Stokes equations (see Cramer and Pai [22]). The electric potential in all directions is assumed to be uniform and the Hall effect of magnetohydrodynamics is neglected. In addition, the effects due to viscous dissipation and Joule heating are assumed to be negligible.

Although this work considers a two-dimensional MHD problem which is somewhat difficult to achieve in a real physical system, a three-dimensional simulation represents the convection phenomenon more realistically. This does not necessarily mean that two-dimensional MHD simulations are of little value but on the contrary, they are less costly from a computational point of view and can provide qualitatively good insight into the convection phenomenon. In general, the interaction of the imposed magnetic field in the x-direction with the y-component of the fluid's velocity will give rise to induced electric currents in the z-direction. In a real three-dimensional problem these currents will close themselves somewhere and will generate a distribution of electric potential. Postulating two-dimensionality as written below and done by previous authors [13, 14, 20, 21] is equivalent to assuming that the electric potential is uniform in the (x, y) plane and throughout the z-direction.

The governing equations for this problem are based on the balance laws of mass, linear momentum, and energy. Taking into account the assumptions mentioned above, and applying the Boussinesq approximation for the body force terms in the momentum equations, the governing equations

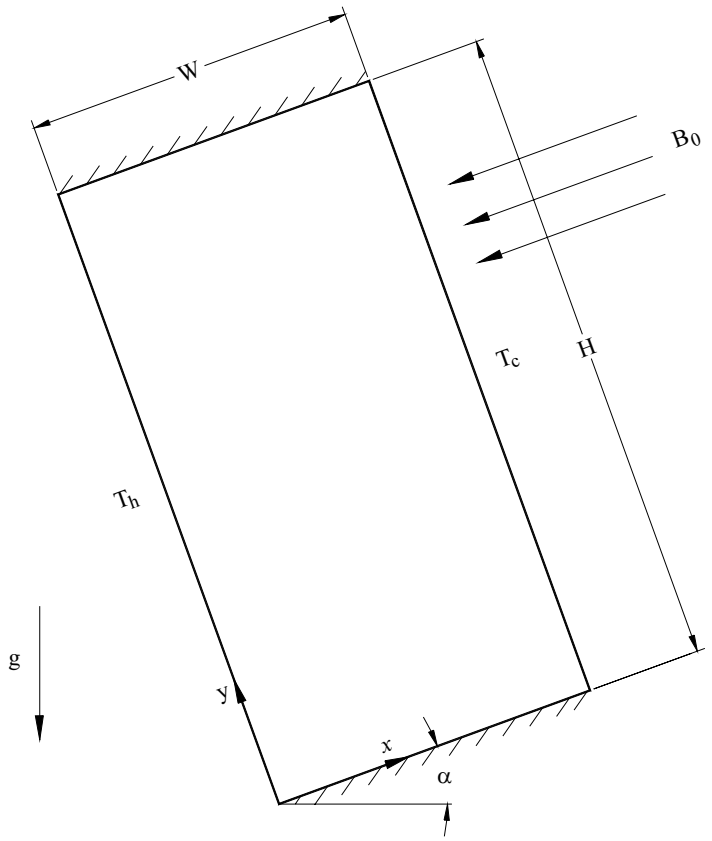

Fig. 1. Schematic diagram of the tilted enclosure with magnetic field.

can be written in dimensional form as

$$\frac{\partial u}{\partial x} + \frac{\partial v}{\partial y} = 0, \tag{1}$$

$$\frac{\partial u}{\partial t} + u\frac{\partial u}{\partial x} + v\frac{\partial u}{\partial y} = -\frac{1}{\rho}\frac{\partial p}{\partial x} + \nu\left(\frac{\partial^2 u}{\partial x^2} + \frac{\partial^2 u}{\partial y^2}\right) + \mathrm{g}\beta_T(T - T_c)\sin\alpha, \tag{2}$$

$$\frac{\partial v}{\partial t} + u\frac{\partial v}{\partial x} + v\frac{\partial v}{\partial y} = -\frac{1}{\rho}\frac{\partial p}{\partial y} + \nu\left(\frac{\partial^2 v}{\partial x^2} + \frac{\partial^2 v}{\partial y^2}\right) + \mathrm{g}\beta_T(T - T_c)\cos\alpha - \frac{\sigma B_0^2}{\rho}\,v, \tag{3}$$

$$\frac{\partial T}{\partial t} + u\frac{\partial T}{\partial x} + v\frac{\partial T}{\partial y} = \alpha_t\left(\frac{\partial^2 T}{\partial x^2} + \frac{\partial^2 T}{\partial y^2}\right), \tag{4}$$

where x, y and t are the distances along and normal to the insulated walls and time, respectively; u, v, p, and T are the velocity components in the x and y-directions, pressure and temperature, respectively. The parameters α_t, ν, β_T, and ρ are the fluid thermal diffusivity, kinematic viscosity, thermal expansion coefficient and density, respectively; σ is the electrical conductivity; B_0 is the magnetic induction; T_h and T_c are the hot and cold wall temperature; α is the enclosure inclination or tilting angle and g is the gravitational acceleration.

The boundary conditions for the problem can be written as

$$\begin{aligned} x=0, \quad y=y: \qquad & u=0, \quad v=0, \quad T=T_h, \\ x=W, \quad y=y: \qquad & u=0, \quad v=0, \quad T=T_c, \\ x=x, \quad y=0: \qquad & u=0, \quad v=0, \quad \frac{\partial T}{\partial y}=0, \\ x=x, \quad y=H: \qquad & u=0, \quad v=0, \quad \frac{\partial T}{\partial y}=0, \end{aligned} \tag{5}$$

where W and H are the width and height of the enclosure, respectively.

The dimensional stream function and vorticity can be defined in the usual way as

$$u=\frac{\partial \Psi}{\partial y}\,, \qquad v=-\frac{\partial \Psi}{\partial x}\,, \qquad \Omega=-\left(\frac{\partial^2 \Psi}{\partial x^2}+\frac{\partial^2 \Psi}{\partial y^2}\right). \tag{6}$$

It is convenient to make Eq. (1) through Eq. (6) dimensionless by using the following dimensionless parameters:

$$\begin{aligned} &\mathrm{X}=\frac{x}{W}\,, && Y=\frac{y}{W}\,, && \tau=\frac{\alpha_t t}{W^2}\,, \\ &\zeta=\frac{\Omega W^2}{\alpha_t}\,, && \psi=\frac{\Psi}{\alpha_t}\,, && \theta=\frac{T-T_c}{T_h-T_c}-0.5\,, \\ &\mathrm{Pr}=\frac{\nu}{\alpha_t}\,, && \mathrm{Ha}=B_0 W\sqrt{\frac{\sigma}{\rho\nu}}\,, && \mathrm{Ra}=\frac{\mathrm{g}\beta_T(T_h-T_c)W^3}{\alpha_t \nu}, \end{aligned} \tag{7}$$

where the dimensionless parameters appearing in the above equations are given in the Nomenclature list.

By employing Eq. (7) and combining Eqs (2) and (3) by eliminating the pressure gradient terms, the resulting dimensionless equations can be written as

$$\zeta=\frac{\partial V}{\partial X}-\frac{\partial U}{\partial Y}=-\nabla^2\psi, \tag{8}$$

$$\begin{aligned} \frac{\partial \zeta}{\partial \tau}+U\frac{\partial \zeta}{\partial X}+V\frac{\partial \zeta}{\partial Y}=\mathrm{Pr}\nabla^2\zeta+\mathrm{Ra}\,\mathrm{Pr}\cos\alpha\left(\frac{\partial \theta}{\partial X}\right) \\ -\mathrm{Ra}\,\mathrm{Pr}\sin\alpha\left(\frac{\partial \theta}{\partial Y}\right)-\mathrm{Ha}^2\mathrm{Pr}\frac{\partial V}{\partial X}\,, \end{aligned} \tag{9}$$

$$\frac{\partial \theta}{\partial \tau}+U\frac{\partial \theta}{\partial X}+V\frac{\partial \theta}{\partial Y}=\nabla^2\theta. \tag{10}$$

The boundary conditions in dimensionless form become

$$Y=0: \qquad U=V=\psi=0, \qquad \zeta=-\left(\frac{\partial^2 \psi}{\partial Y^2}\right), \qquad \frac{\partial \theta}{\partial Y}=0, \tag{11a}$$

$$Y = H/W: \qquad U = V = \psi = 0, \qquad \zeta = -\left(\frac{\partial^2 \psi}{\partial Y^2}\right), \qquad \frac{\partial \theta}{\partial Y} = 0, \tag{11b}$$

$$X = 0: \qquad U = V = \psi = 0, \qquad \zeta = -\left(\frac{\partial^2 \psi}{\partial X^2}\right), \qquad \theta = 0.5, \tag{11c}$$

$$X = 1: \qquad U = V = \psi = 0, \qquad \zeta = -\left(\frac{\partial^2 \psi}{\partial X^2}\right), \qquad \theta = -0.5. \tag{11d}$$

The average Nusselt number at the heated wall of the enclosure are given by

$$\overline{\mathrm{Nu}} = -\frac{1}{A}\int_0^A \frac{\partial \theta}{\partial X}\, dY, \tag{12}$$

where $A = H/W$ is the enclosure aspect ratio.

2. Numerical Algorithm

The numerical algorithm used to solve Eq. (8) through Eq. (10) is based on the finite-difference methodology. Central difference quotients were used to approximate the second derivatives in both the X and Y-directions while the time derivative is approximated by a two-point backward difference formula. The governing equations are then transformed into tri-diagonal algebraic equations that were solved in the X and Y-directions for the temperature, vorticity and the stream function at different time steps. This method was found to be stable.

As an example, the finite-difference formulation for Eq. (10) takes on the form

$$\begin{aligned}
&\frac{\left[\zeta_{i,j}^{n+1} - \zeta_{i,j}^{n}\right]}{\Delta\tau} + U_{i,j}\frac{\left[\zeta_{i+1,j}^{n+1} - \zeta_{i-1,j}^{n+1}\right]}{2\Delta X} + V_{i,j}\frac{\left[\zeta_{i,j+1}^{n} - \zeta_{i,j-1}^{n}\right]}{2\Delta Y} \\
&= \mathrm{Pr}\left\{\frac{\left[\zeta_{i+1,j}^{n+1} - 2\zeta_{i,j}^{n+1} + \zeta_{i-1,j}^{n+1}\right]}{\Delta X^2} + \frac{\left[\zeta_{i,j+1}^{n} - 2\zeta_{i,j}^{n+1} + \zeta_{i,j-1}^{n}\right]}{\Delta Y^2}\right\} \\
&+ \mathrm{Ra}\,\mathrm{Pr}\cos\alpha\frac{\left[\theta_{i+1,j} - \theta_{i-1,j}\right]}{2\Delta X} - \mathrm{Ra}\,\mathrm{Pr}\sin\alpha\frac{\left[\theta_{i,j+1} - \theta_{i,j-1}\right]}{2\Delta Y} \\
&- \mathrm{Ha}^2\mathrm{Pr}\frac{\left[V_{i+1,j} - V_{i-1,j}\right]}{2\Delta X},
\end{aligned} \tag{13}$$

which can be rearranged as

$$\zeta_{i-1,j}^{n+1}\left[E_1\right] + \zeta_{i,j}^{n+1}\left[B_1\right] + \zeta_{i+1,j}^{n+1}\left[A_1\right] = \left[D_1\right], \tag{14}$$

where

$$E_1 = \left[-\frac{U_{i,j}\Delta\tau}{2\Delta X} - \frac{\mathrm{Pr}\Delta\tau}{\Delta X^2} \right];$$

$$B_1 = \left[1.0 + \frac{2\mathrm{Pr}\Delta\tau}{\Delta X^2} + \frac{2\mathrm{Pr}\Delta\tau}{\Delta Y^2} \right]; \qquad A_1 = \left[\frac{U_{i,j}\Delta\tau}{2\Delta X} - \frac{\mathrm{Pr}\Delta\tau}{\Delta X^2} \right];$$

$$D_1 = \zeta^n_{i,j+1} \left[-\frac{V_{i,j}\Delta\tau}{2\Delta Y} + \frac{\mathrm{Pr}\Delta\tau}{\Delta Y^2} \right] + \zeta^n_{i,j} \left[1.0 \right] + \zeta^n_{i,j-1} \left[\frac{V_{i,j}\Delta\tau}{2\Delta Y} + \frac{\mathrm{Pr}\Delta\tau}{\Delta Y^2} \right] \tag{15}$$

$$+ \mathrm{Ra}\,\mathrm{Pr}\Delta\tau\cos\alpha\frac{[\theta_{i+1,j} - \theta_{i-1,j}]}{2\Delta X} - \mathrm{Ra}\,\mathrm{Pr}\Delta\tau\sin\alpha\frac{[\theta_{i,j+1} - \theta_{i,j-1}]}{2\Delta Y}$$

$$- \mathrm{Ha}^2\,\mathrm{Pr}\,\Delta\tau\,\frac{[V_{i+1,j} - V_{i-1,j}]}{2\Delta X}.$$

All other equations and the boundary conditions are discretized in the same way. The subscripts i and j denote the X and Y locations whereas superscripts n and $n+1$ denote the time step, respectively. In the present study, the numerical computations were carried out for 61×81 grid nodal points with a time step of 10^{-5} and step sizes $\Delta X = 1/60$ and $\Delta Y = 1/80$ in the X and Y-directions, respectively. The time marching procedure is used herein as one of the possible numerical schemes to achieve a converged stationary solution. At each specific time, the convergence criterion required that the difference between the current and previous iterations for all of the dependent variables be 10^{-4}. In all the results obtained, the enclosure aspect ratio A was taken to be equal to 2.

3. Results and Discussion

In this section, numerical results for the streamline and temperature contours as well as selected velocity and temperature profiles at mid-section of the enclosure for various values of the Hartmann number Ha, inclination angle α and Rayleigh number Ra will be reported. In addition, representative results for the average Nusselt number $\overline{\mathrm{Nu}}$ at various conditions will be presented and discussed. These results correspond to convective flow of liquid gallium ($\mathrm{Pr} = 0.025$) or germanium ($\mathrm{Pr} = 0.007$) confined in a rectangular cavity or enclosure of aspect ratio of 2 subject to a transverse temperature gradient across the non-adiabatic walls of the enclosure. Both gallium and germanium are used in the semiconductor industry in addition to other uses. Each has several unique properties. For example, gallium melts at a relatively low temperature, and liquid gallium can remain in the liquid state below its melting temperature for considerable periods of time. It also has a very large temperature range (from $29.78^\circ\mathrm{C}$ to $2403.0^\circ\mathrm{C}$) over which it can remain liquid. This characteristic makes it useful for high temperature thermometers, pressure gauges, and as a high-temperature lubricant. Gallium is magnetic and is an excellent conductor of heat and electricity. Unlike most materials, gallium expands upon freezing, so that it cannot be stored in metal, ceramic or other rigid containers. Tables 1 and 2 give the thermophysical properties of gallium and germanium, respectively. As mentioned before, the origin of this problem lies in the area of crystal growth where it is known that the motion of the fluid in semiconductor geometries is of vital importance in determining the quality of the crystal. In recent years, strong magnetic fields have been used in crystal growth of semiconductor materials in order to reduce macroscopic inhomogeneity in the crystal by suppression of buoyancy-driven convection (see [23, Chapter 4]). It is well known by now that the homogeneity of crystals can be drastically influenced by imposed magnetic fields.

Table 1
Thermophysical properties of gallium.

Thermal conductivity	$\mathrm{W}/^{\circ}\mathrm{C}\cdot\mathrm{cm}$	0.29
Density	g/cm^3	6.09
Specific heat	$\mathrm{J}/^{\circ}\mathrm{C}\cdot\mathrm{g}$	0.37
Melting temperature	$^{\circ}\mathrm{C}$	29.78
Kinematic viscosity	cm^2/s	0.0033
Thermal expansion coefficient	$^{\circ}\mathrm{C}^{-1}$	$1.2\cdot 10^{-4}$

Table 2
Thermophysical properties of germanium.

Thermal conductivity	$\mathrm{W}/^{\circ}\mathrm{C}\cdot\mathrm{cm}$	0.39
Density	g/cm^3	5.50
Specific heat	$\mathrm{J}/^{\circ}\mathrm{C}\cdot\mathrm{g}$	0.39
Melting temperature	$^{\circ}\mathrm{C}$	937.4
Kinematic viscosity	cm^2/s	0.0013
Thermal expansion coefficient	$^{\circ}\mathrm{C}^{-1}$	$5\cdot 10^{-4}$

Fig. 2 presents steady-state contour plots for the streamline and temperature for various values of the Hartmann number Ha for $\mathrm{Pr}=0.025$, $\mathrm{Ra}=10^5$ and $\alpha=45^{\circ}$. In the absence of a magnetic field ($\mathrm{Ha}=0$) the streamline contours exhibit a unique feature where three recirculating cells with non-uniform temperature contours are predicted within the enclosure. A primary cell exists in the core of the enclosure while two secondary cells occur one close to each of the insulated walls of the enclosure. On the other hand, for a relatively lower strength magnetic field ($\mathrm{Ha}=30$), this feature does not exist and a single recirculation cell is predicted within the enclosure with the temperature contours being crowded close to the walls of the enclosure and being some what uniform in the core region. However, as the strength of the magnetic field increases, the streamline contours become non-uniform, more stretched and distorted and the flow moves slower. This is evident from the decreases in the absolute value of the stream function as Ha increases. The distortion effect which occurs in the clock-wise direction continues as Ha becomes equal to 70 causing the formation of two recirculation cells, one close to each of the two insulated walls. As the strength of the magnetic field is increased further until Ha reaches 100, the streamlines get stretched more and the two recirculation cells move closer and closer to the insulated walls. Also, the temperature contours tend to become more parallel to the longer walls of the enclosure indicating the approach to a quasi-conduction regime. In addition, the non-uniform behavior of the temperature contours for $\mathrm{Ha}=70$ due to the formation of the two recirculating cells is obvious from Fig. 2. It can be concluded that the main contributions of the presence of the magnetic field are predicted to be a flow retardation effect, formation of two-cellular vortices and a suppression of the overall heat transfer in the enclosure.

Fig. 3 through Fig. 5 depict the effects of the Hartmann number Ha on the X-component of velocity, Y-component of velocity and temperature profiles, respectively. It is known by now that application of a magnetic field to an electrically-conducting fluid tends to slow down the movement of the fluid and to produce increases in the fluid temperature. This is clearly obvious from Fig. 3 through Fig. 5 where the net velocity decreases while the temperature near the hot wall increases as the Hartmann number increases. Due to the existence of two-cellular vortices as discussed before, the X-component of velocity tends to behave in a non-uniform manner as Ha increases. However,

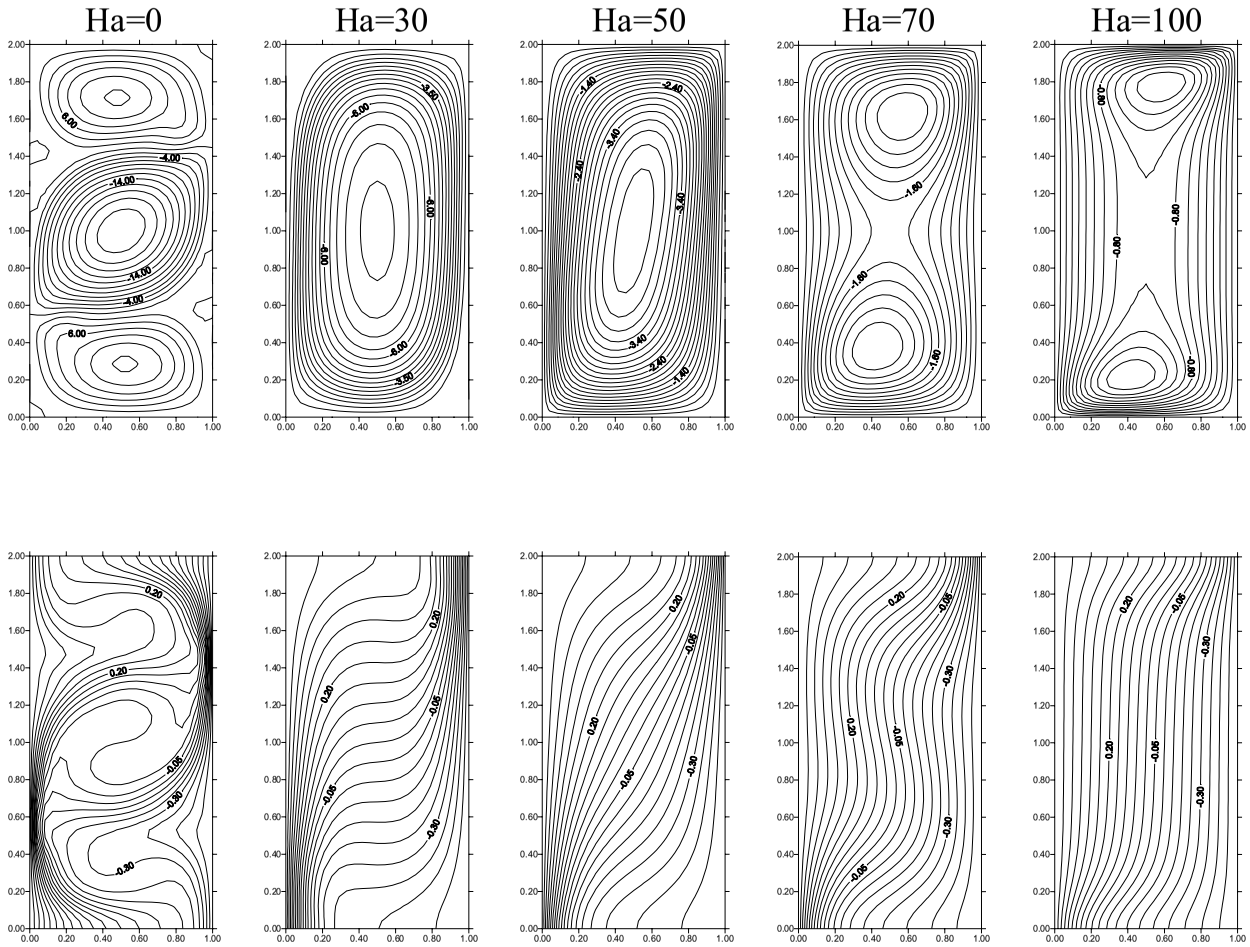

Fig. 2. Effects of Hartmann number on streamlines (a) and isotherms (b), $\mathrm{Pr} = 0.025$, $\mathrm{Ra} = 10^5$, and $\alpha = 45^\circ$.

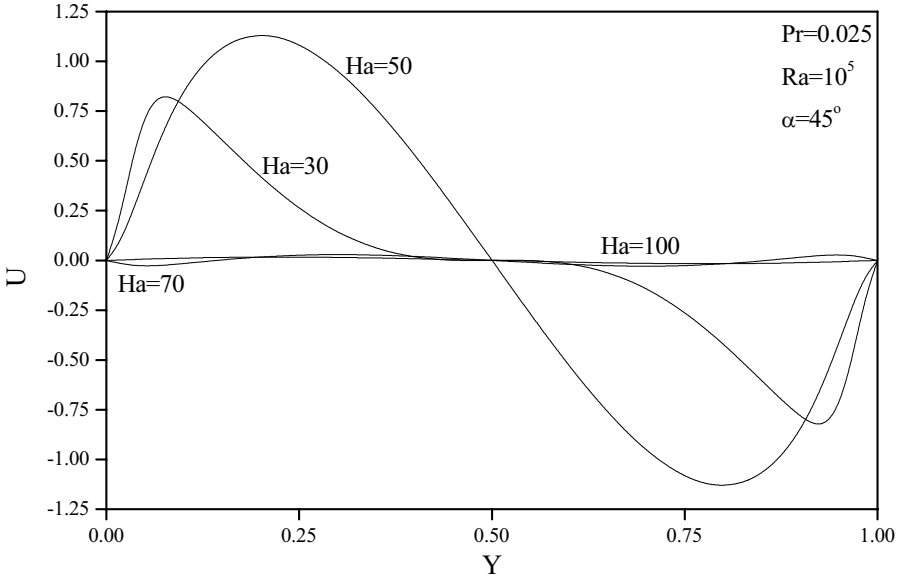

Fig. 3. Effects of Ha on X-component of velocity at enclosure mid-section.

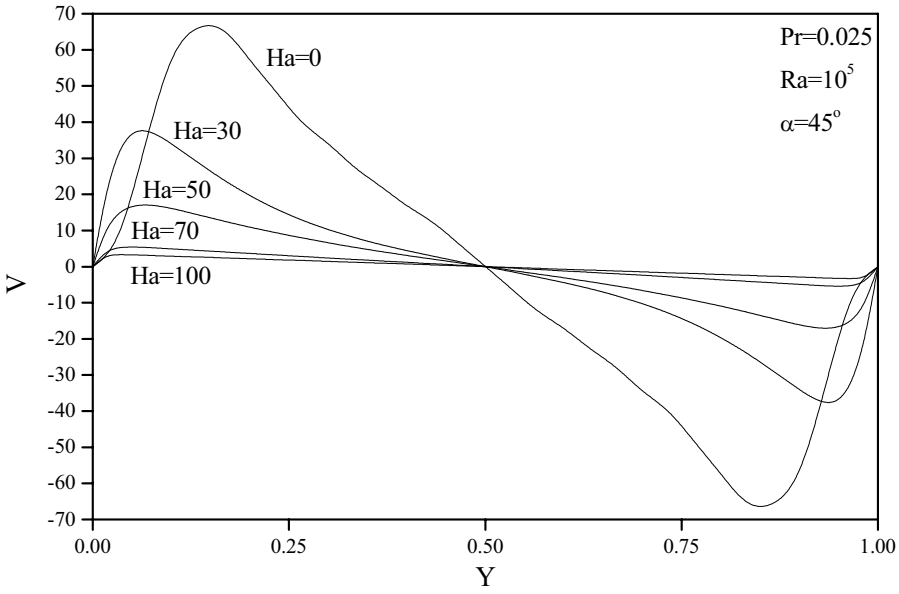

Fig. 4. Effects of Ha on Y-component of velocity at enclosure mid-section.

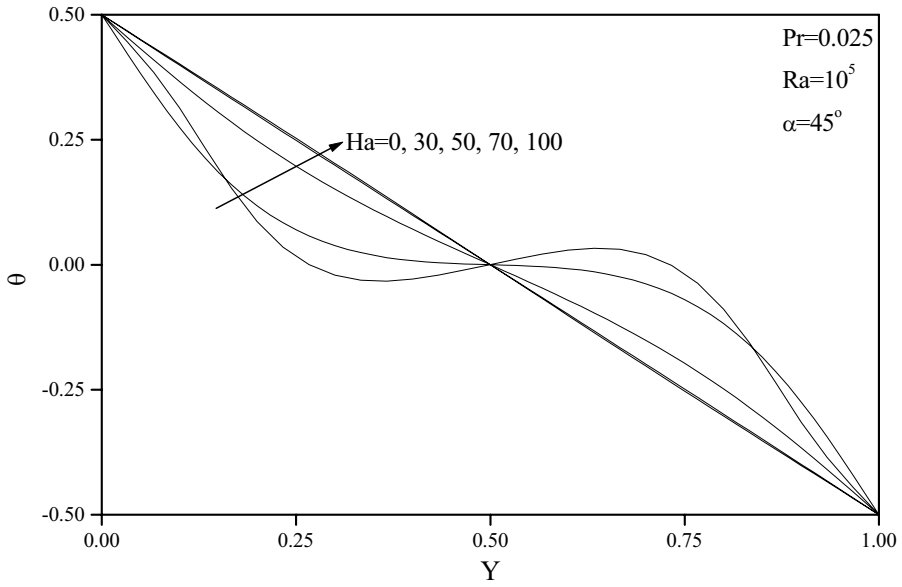

Fig. 5. Effects of Ha on temperature profiles at enclosure mid-section.

the net magnitude of the velocity field decreases as the strength of the magnetic field increases.

Fig. 6 illustrates the effects of the enclosure inclination angle α on the contours of the streamlines and temperature for $\mathrm{Ha} = 70$, $\mathrm{Pr} = 0.025$, and $\mathrm{Ra} = 10^5$. For $\alpha = 0^\circ$ (non-inclined vertical enclosure) a single stretched recirculating cell or vortex in the whole enclosure exists. As the enclosure is tilted by 30°, two connected vortices within the enclosure, one close to each of the insulated walls are predicted. Further tilting of the enclosure until $\alpha = 45^\circ$, the two vortices become more distinctive. However, when the enclosure inclination angle becomes 60° a third small vortex starts to form within the core of the enclosure. A more systematic and interesting behavior is that corresponding to $\alpha = 90^\circ$. For this case four separated recirculating cells are predicted. For $\alpha = 0^\circ$ the isotherms are crowded away from the core region of the enclosure and are some what parallel to the non-insulated walls. For $\alpha = 30^\circ$ they become more parallel in the core region. However, for $\alpha > 30^\circ$ the isotherms show significant non-uniform behavior in the boundary-layer regions close to the walls as well as in the enclosure core region. This type of behavior is associated with the existence of multiple interacting vortices as discussed before. In general, it is predicted that inclination of the enclosure has the effect of exhibiting a multi-cellular structure. The number of recirculating cells is a function of the enclosure inclination angle for the same parametric values of Ha, Pr and Ra.

Figs 7 through 9 present representative profiles for the fluid X-component of velocity U, Y-component of velocity V and temperature θ at mid-section of the enclosure for various enclosure inclination angles α, respectively. For $\alpha = 0^\circ$ (non-inclined vertical enclosure), due to the effect of buoyancy, an upward fluid flow along the hot wall is induced while a backward flow takes place along the cold wall. As the enclosure is tilted, it becomes harder for the fluid to move along the walls resulting in less induced flow. This is depicted in the reductions in both the X and Y-components of velocity as α increases. However, for $\alpha = 90^\circ$, the fluid speed seems to increase significantly. This is associated with the fact that the contribution of the X-component of temperature gradient (buoyancy effect) does not affect the flow since it is multiplied by $\cos\alpha$ which vanishes for $\alpha = 90^\circ$. It should be mentioned that in Fig. 7, the line corresponding to $\alpha = 90^\circ$ is not shown because it

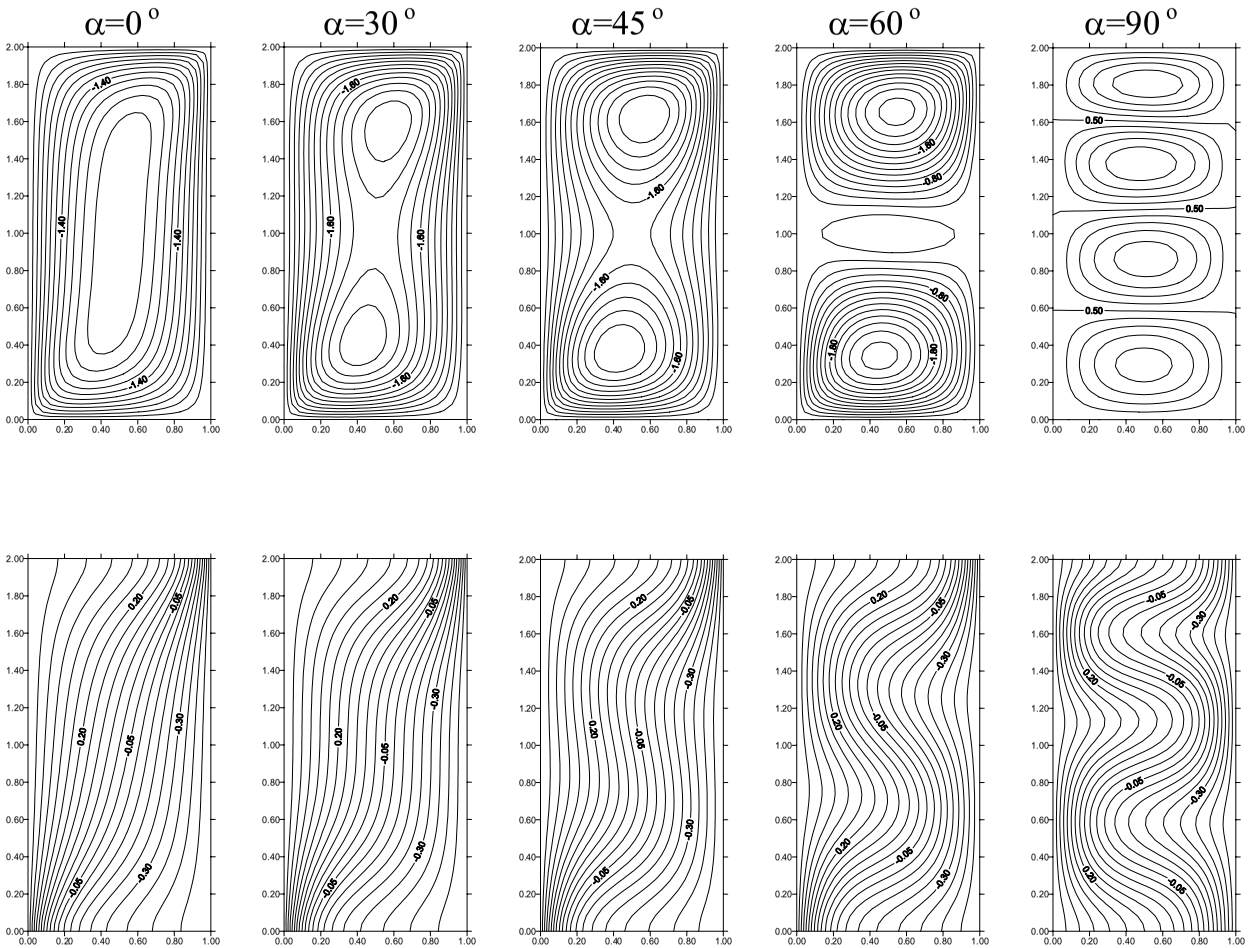

Fig. 6. Effects of enclosure inclination angle on streamlines (a) and isotherms (b), $\mathrm{Ha} = 70$, $\mathrm{Pr} = 0.025$, and $\mathrm{Ra} = 10^5$.

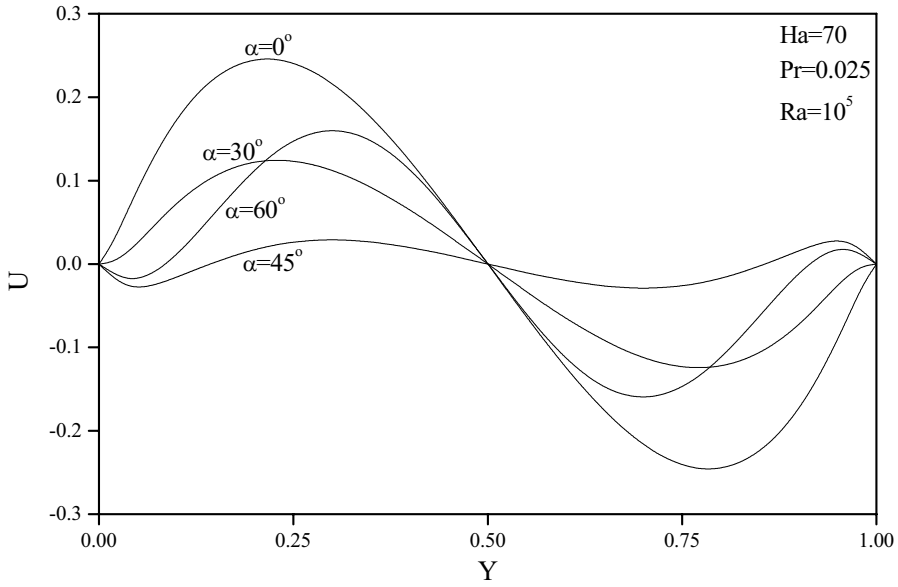

Fig. 7. Effects of α on X-component of velocity at enclosure mid-section.

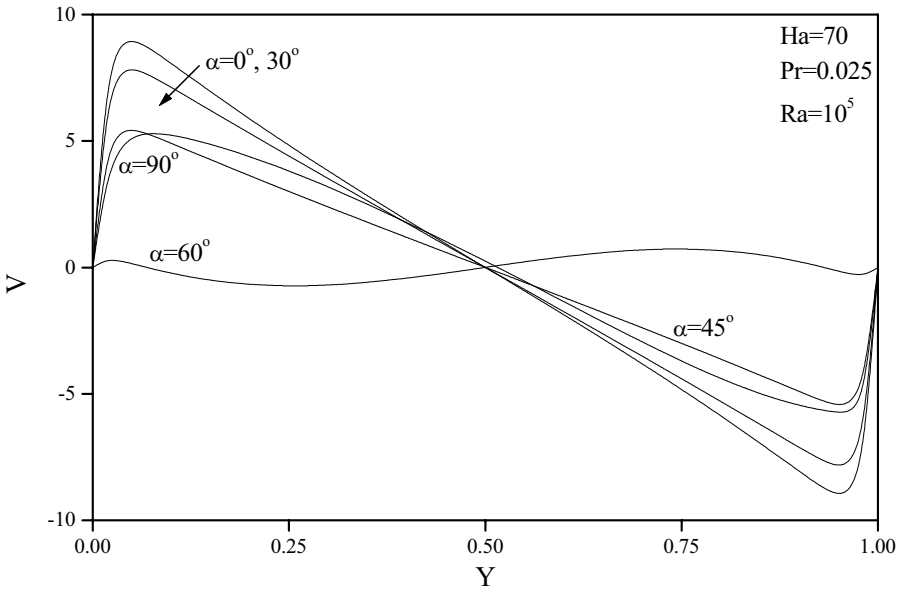

Fig. 8. Effects of α on Y-component of velocity at enclosure mid-section.

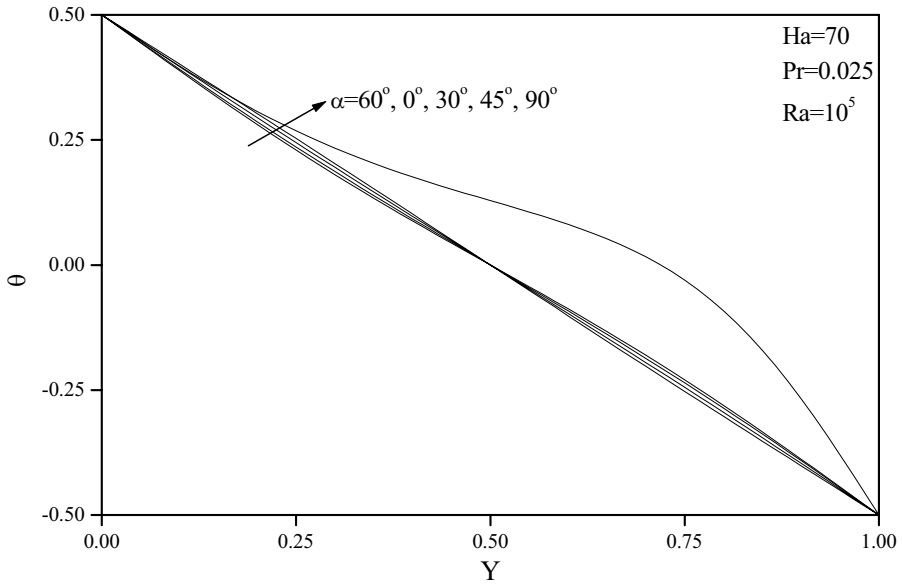

Fig. 9. Effects of α on temperature profiles at enclosure mid-section.

falls significantly outside the scale of the figure. As for the temperature profiles, they show a trend for which they initially increase close to the hot wall as α is increased from 0° to 45° and then they decrease for $\alpha = 60^\circ$ and then they finally increase again for $\alpha = 90^\circ$. This behavior is probably associated with the formation of multiple circulation cells for an inclined enclosure as was shown in Fig. 6.

Fig. 10 illustrates the influence of the enclosure inclination angle α on the contours of the streamlines and temperature for liquid gallium ($\mathrm{Pr} = 0.025$) with $\mathrm{Ha} = 70$ and $\mathrm{Ra} = 10^6$. By comparison with Fig. 6, it can be seen that a clearly different behavior is predicted. Unlike the case for $\mathrm{Ra} = 10^5$, a single dominating recirculting cell exists for all enclosure inclination angles up to $\alpha = 60^\circ$. However, for $\alpha = 90^\circ$, a tri-cellular structure is predicted. Between $\alpha = 0^\circ$ and $\alpha = 60^\circ$, the effect of enclosure inclination is limited to stretching and increasing the domain of influence of the single cell within the enclosure. These behaviors in the streamline contours are clearly shown in Fig. 10 and they affect the contour maps of temperature accordingly. In general, the isotherms exhibit different features than those discussed previously in Fig. 6. In this case, the convection effect dominates and the isotherms are nearly uniform in the core region for all angles up to $\alpha = 60^\circ$ and the non-uniform behavior discussed previously is limited to the case corresponding to $\alpha = 90^\circ$ where three distinctive vortices exist.

Figs 11 through 13 show the effects of α on the profiles of the fluid X-component of velocity, Y-component of velocity and temperature at mid-section of the enclosure for the same parameters as in Figs 7 through 9 but $\mathrm{Ra} = 10^6$, respectively. By comparison with Figs 7 through 9, it can be easily seen that, as expected, the induced flow velocities for this case are much higher. In general, both the X and Y-components of velocity decrease in the immediate vicinity of the hot wall as α increases. However, for $\alpha = 90^\circ$, the fluid speed seems to increase significantly above that for $\alpha = 60^\circ$. Again, this is related to elimination of the contribution of the X-component of the buoyancy force for $\alpha = 90^\circ$. Again, in Fig. 11, the line corresponding to $\alpha = 90^\circ$ is not shown because it falls significantly outside the scale of the figure. As for the temperature profiles in Fig. 13, they show a trend for which they initially decrease close to the hot wall as α is increased from 0°

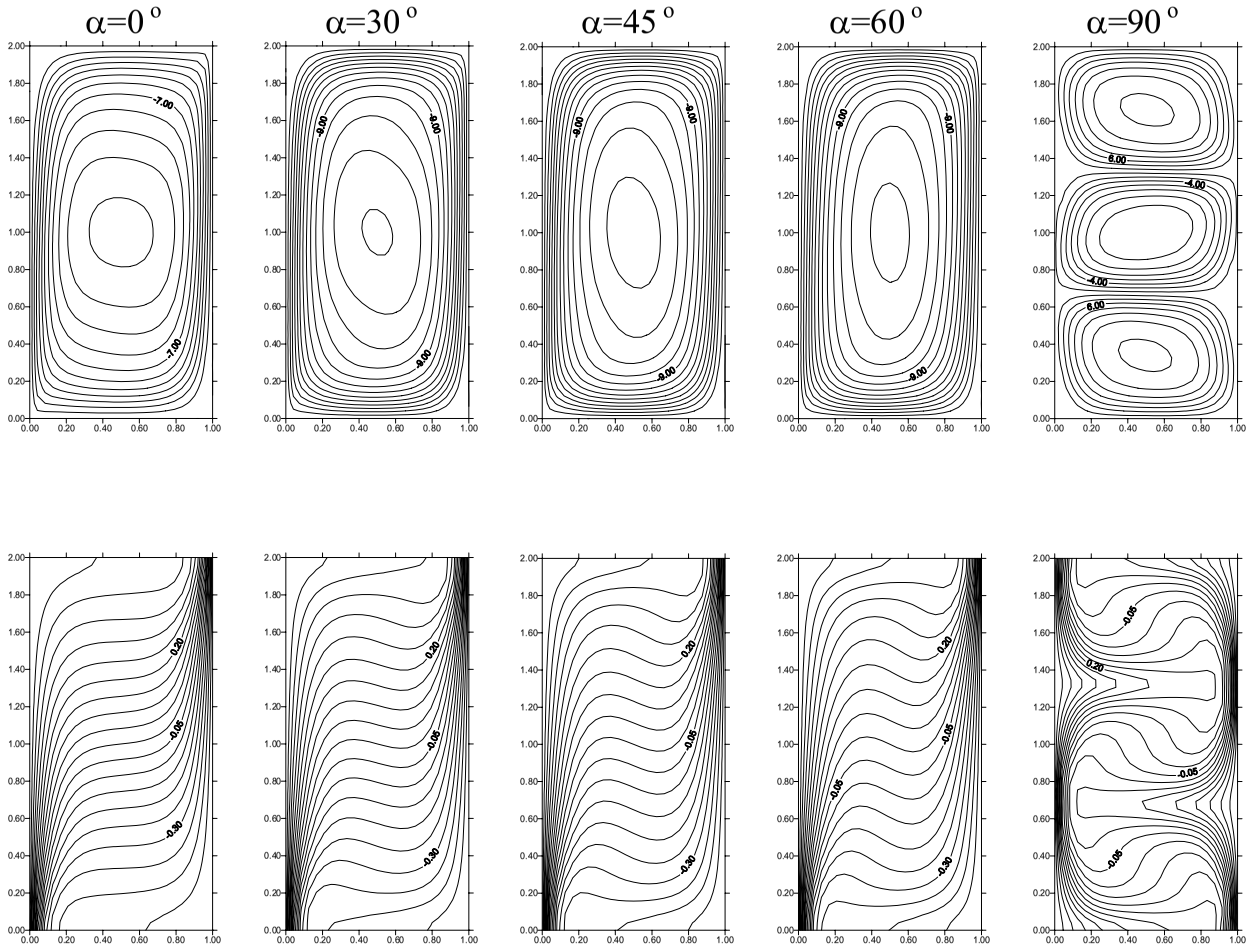

Fig. 10. Effects of enclosure inclination angle on streamlines (a) and isotherms (b), $\mathrm{Ha} = 70$, $\mathrm{Pr} = 0.025$, and $\mathrm{Ra} = 10^6$.

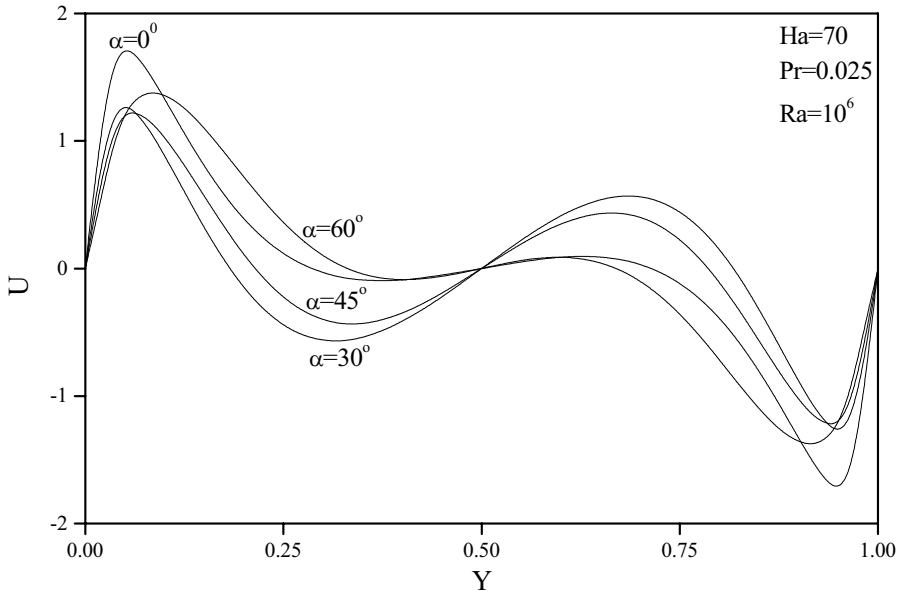

Fig. 11. Effects of α on X-component of velocity at enclosure mid-section.

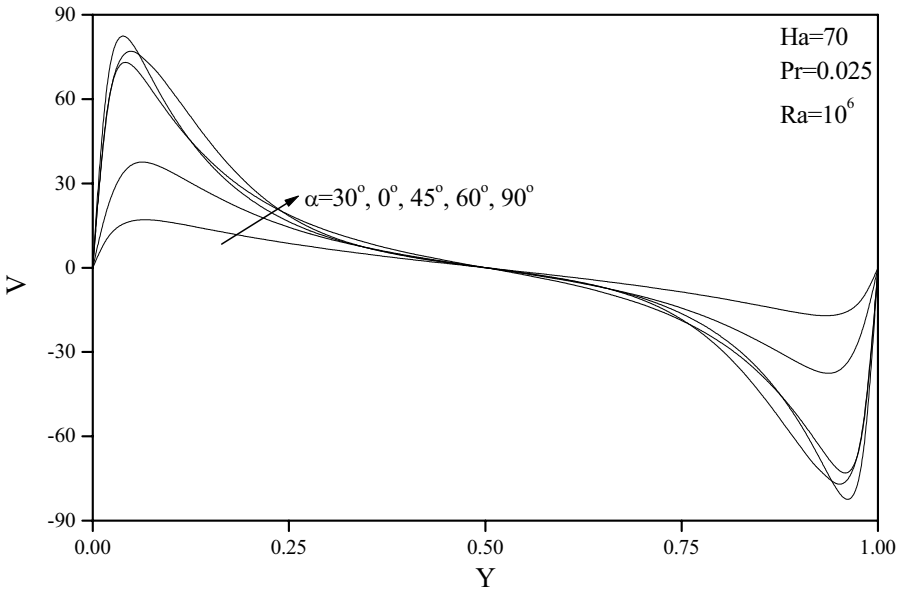

Fig. 12. Effects of α on Y-component of velocity at enclosure mid-section.

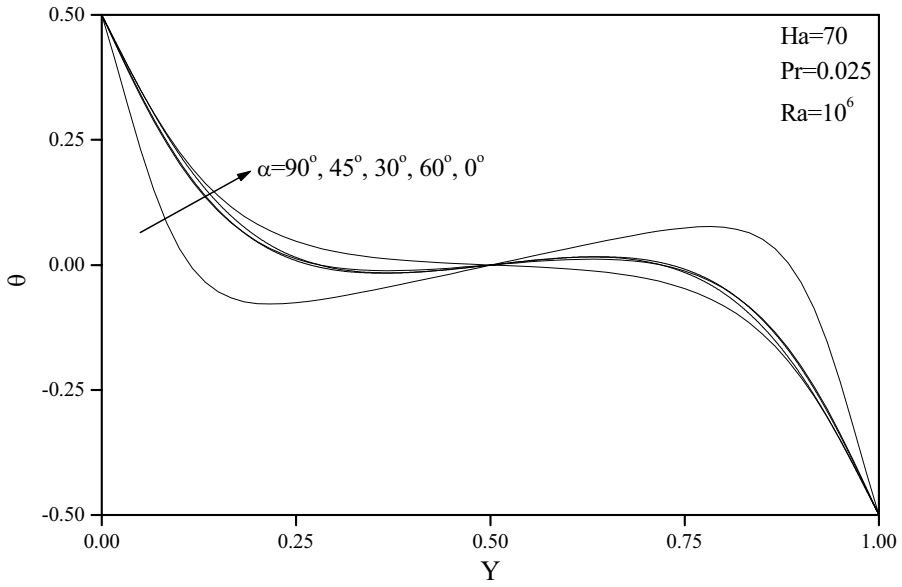

Fig. 13. Effects of α on temperature profiles at enclosure mid-section.

to 45° and then they increase for $\alpha = 60^\circ$ and then they finally decrease again for $\alpha = 90^\circ$. This behavior is exactly the opposite as that seen in Fig. 9 and this is related to the different isotherms behavior predicted in both Figs 6 and 10 in which conduction is dominant in the former while convection is dominant in the latter.

In Fig. 14, the streamline and temperature contours are shown for germanium liquid metal ($\mathrm{Pr} = 0.007$) at various enclosure inclination angles with $\mathrm{Ha} = 70$ and $\mathrm{Ra} = 10^5$. It is interesting to observe in this case the development of the streamlines from a single recirculating cell for $\alpha = 0^\circ$ and $\alpha = 30^\circ$ to bi-cellular structure for $\alpha = 45^\circ$ and $\alpha = 60^\circ$ and then a tri-cellular structure for $\alpha = 90^\circ$ with increased stretching and distortion effects as α is increased. The isotherms show a similar trend as those presented in Fig. 6 for gallium ($\mathrm{Pr} = 0.0025$). They are crowded away from the core region of the enclosure and are some what parallel to the non-adiabatic walls and they become more parallel to these walls in the core region as α increases up to $\alpha = 60^\circ$. However, for $\alpha = 90^\circ$ the isotherms show a significant non-uniform behavior in the boundary-layer regions close to the walls as well as in the enclosure core region. Again, this is associated with the existence of a tri-cellular streamlines structure as mentioned before.

Figs 15 through 17 present the effects of α on the profiles of U, V, and θ at the enclosure mid-section for germanium ($\mathrm{Pr} = 0.007$) at $\mathrm{Ha} = 70$ and $\mathrm{Ra} = 10^5$, respectively. Unlike the case of gallium ($\mathrm{Pr} = 0.025$), the profiles of U increase with increasing values of α up to $\alpha = 60^\circ$ and then decreases for $\alpha = 90^\circ$. However, the profiles of V behave in the same way as those of gallium where they decrease with increasing values of α up to $\alpha = 60^\circ$ and then they increase $\alpha = 90^\circ$ for the reasons mentioned before. The temperature profiles show that the temperature near the hot wall increases with increases in the values of α up to $\alpha = 60^\circ$ and then decreases for $\alpha = 90^\circ$.

The effects of the Hartmann number Ha on the average Nusselt number $\overline{\mathrm{Nu}}$ at the hot wall of the enclosure and the absolute maximum and minimum stream function values (extrema) $|\psi_{\max}|$ and $|\psi_{\min}|$ for liquid gallium ($\mathrm{Pr} = 0.025$) at $\mathrm{Ra} = 10^5$ and $\alpha = 45^\circ$ are presented in Table 3. In the absence of magnetic field, the values of $\overline{\mathrm{Nu}}$, $|\psi_{\max}|$ and $|\psi_{\min}|$ are large. Application of the magnetic field has the tendency to decrease the negative temperature gradient at the hot wall

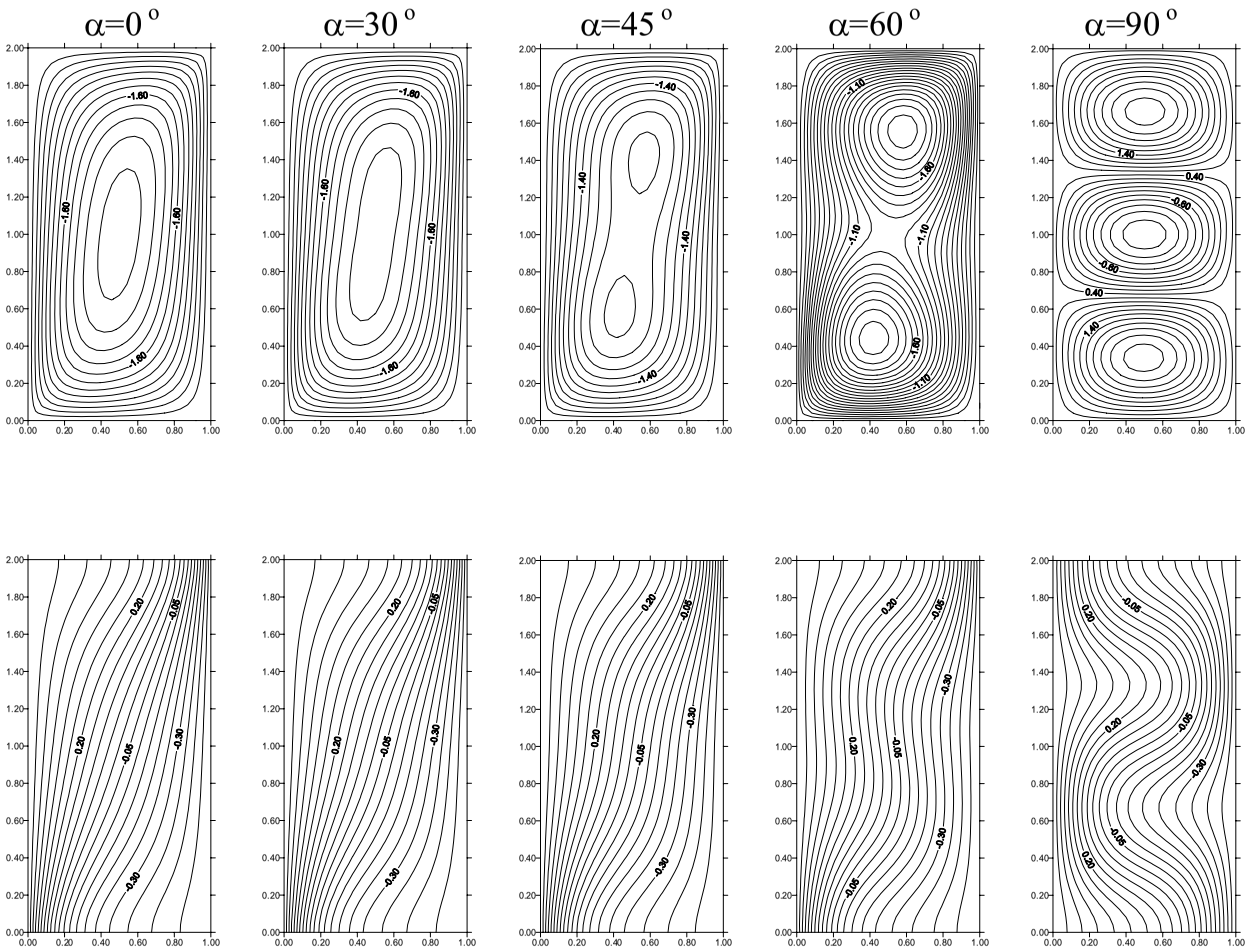

Fig. 14. Effects of enclosure inclination angle on streamlines (a) and isotherms (b), $\mathrm{Ha} = 70$, $\mathrm{Pr} = 0.007$, and $\mathrm{Ra} = 10^5$.

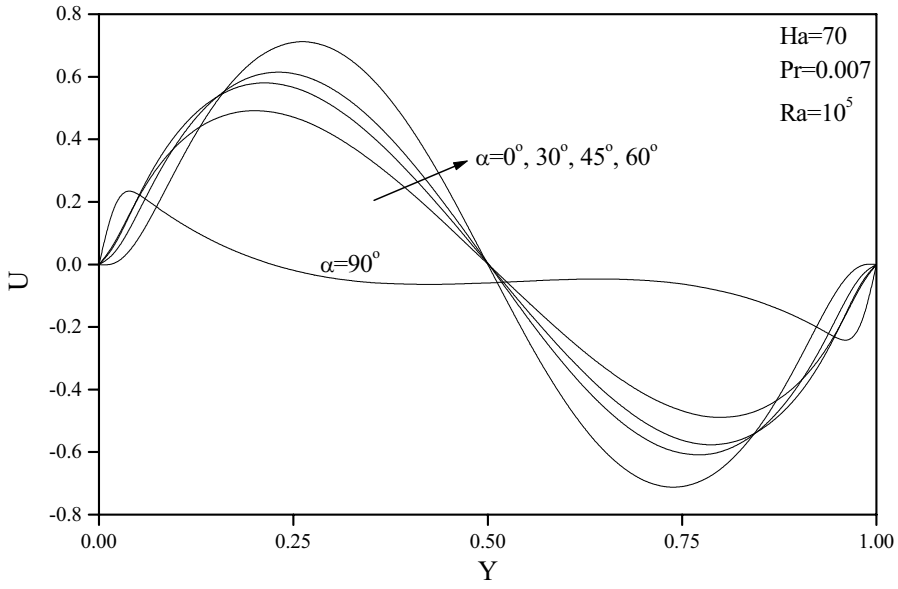

Fig. 15. Effects of α on X-component of velocity at enclosure mid-section.

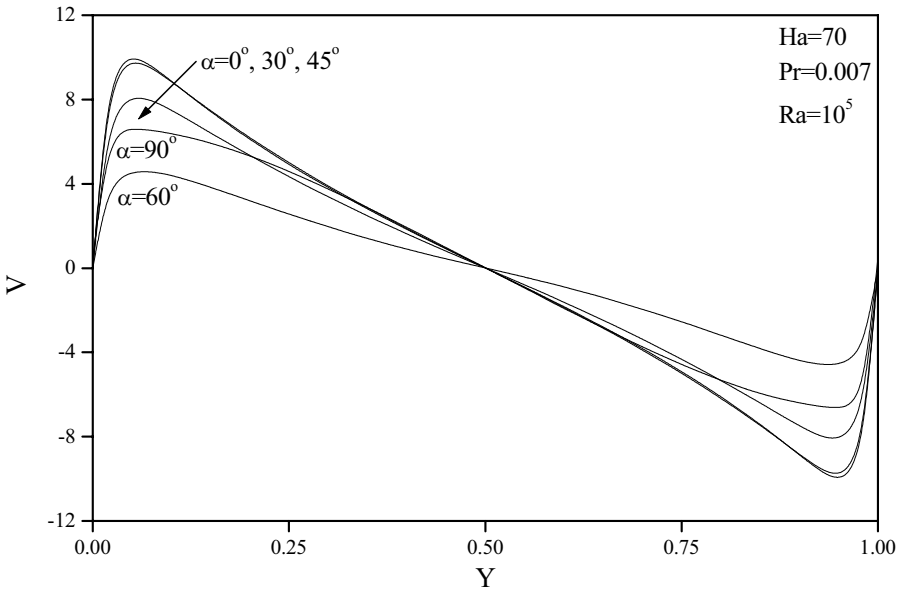

Fig. 16. Effects of α on Y-component of velocity at enclosure mid-section.

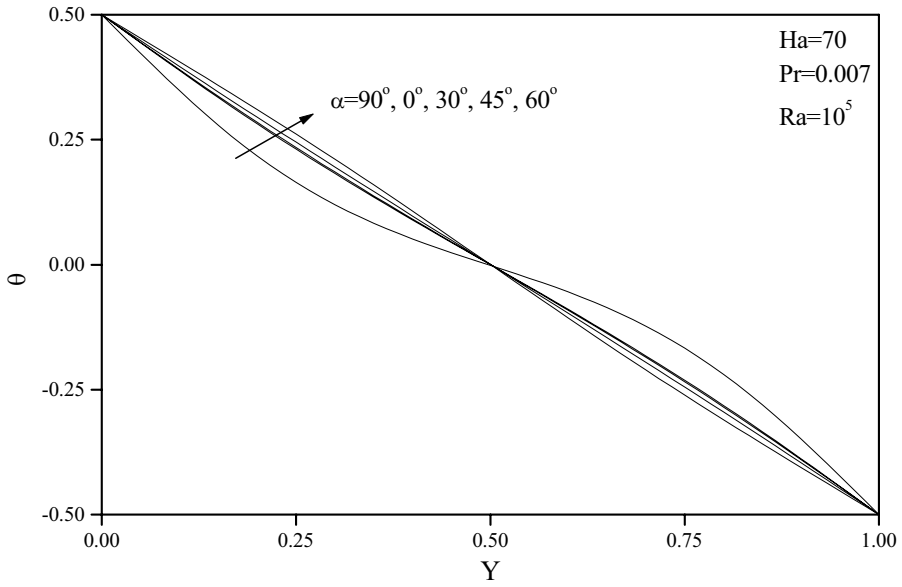

Fig. 17. Effects of α on temperature profiles at enclosure mid-section.

resulting in significant reductions in $\overline{\mathrm{Nu}}$. As the strength of the magnetic field increases further, the values of $\overline{\mathrm{Nu}}$ decrease further. In addition, while the values of the maximum stream function remain unchanged (for $\mathrm{Ha} > 0$), the absolute minimum values tend to decrease with increasing values of the Hartmann number. These behaviors are clearly obvious in Table 3.

Table 4 depicts the influence of the enclosure inclination angle α on the values of the average Nusselt number $\overline{\mathrm{Nu}}$ at the hot wall of the enclosure and the absolute maximum and minimum stream function values $|\psi_{\max}|$ and $|\psi_{\min}|$ for liquid gallium ($\mathrm{Pr} = 0.025$) at $\mathrm{Ha} = 70$ and $\mathrm{Ra} = 10^5$. In general, it is observed that the values of $\overline{\mathrm{Nu}}$ increase with increasing values of α except for $\alpha = 45^\circ$ where a slight decrease in the value of $\overline{\mathrm{Nu}}$ indicating a minimum is predicted. This is probably related to the beginning of the non-uniform behavior in the isotherms are reported in Fig. 6. In addition, tilting the enclosure up to $\alpha = 45^\circ$ causes $|\psi_{\min}|$ to increase reaching a maximum while $|\psi_{\max}|$ remains unchanged. However, as α is increased beyond 45°, the values of $|\psi_{\max}|$ increase significantly while the values of $|\psi_{\min}|$ decrease beyond $\alpha = 60^\circ$. This behavior is related to the formation of multi-cellular streamline structure for high values of α as discussed before.

Table 5 presents the same properties as in Table 4 except for $\mathrm{Ra} = 10^6$. In comparison with Table 4, it is seen that the values of $\overline{\mathrm{Nu}}$, $|\psi_{\max}|$ and $\psi_{\min}|$ increase as Ra increases. This is expected since the convection heat transfer due to thermal buoyancy effects in the enclosure increases as the Rayleigh number increases. In addition, it is observed that a non-uniform behavior in the values of $\overline{\mathrm{Nu}}$ takes place in which they increase as α increases up to $\alpha = 30^\circ$ and then they decrease for $\alpha = 45^\circ$ and $\alpha = 60^\circ$ and finally increase significantly for $\alpha = 90^\circ$ where a tri-cellular streamline structure and an irregular isotherm trend occur. Furthermore, the value of $|\psi_{\max}$ remains unchanged at the value of zero as the enclosure is tilted from the vertical position ($\alpha = 0^\circ$) to $\alpha = 60^\circ$ and it increases significantly for $\alpha > 60^\circ$. However, the value of $|\psi_{\min}|$ increases with increasing values of α up to $\alpha = 45^\circ$ and decreases for $\alpha = 60^\circ$ and then it increases again for $\alpha = 90^\circ$.

Finally, Table 6 shows the effects of α on the values of $\overline{\mathrm{Nu}}$ for germanium ($\mathrm{Pr} = 0.007$) at $\mathrm{Ha} = 70$ and $\mathrm{Ra} = 10^5$. By comparison with the case of gallium ($\mathrm{Pr} = 0.025$) in Table 4, it is seen

Table 3
Effects of Hartmann number on the average Nusselt and the absolute maximum and minimum stream function values for $\mathrm{Pr} = 0.025$, $\mathrm{Ra} = 10^5$ and $\alpha = 45^\circ$.

Parameter	$\overline{\mathrm{Nu}}$	$\lvert\psi_{\max}\rvert$	$\lvert\psi_{\min}\rvert$
$\mathrm{Ha} = 0$	4.61902	12.25007	23.77266
$\mathrm{Ha} = 30$	2.77555	0.00000	8.19003
$\mathrm{Ha} = 50$	1.86365	0.00000	4.33063
$\mathrm{Ha} = 70$	1.42970	0.00000	2.59826
$\mathrm{Ha} = 100$	1.13567	0.00000	1.29340

Table 4
Effects of enclosure inclination angle on the average Nusselt and the absolute maximum and minimum stream function values for $\mathrm{Ha} = 70$, $\mathrm{Pr} = 0.025$, and $\mathrm{Ra} = 10^5$.

Parameter	$\overline{\mathrm{Nu}}$	$\lvert\psi_{\max}\rvert$	$\lvert\psi_{\min}\rvert$
$\alpha = 0^\circ$	1.40251	0.00000	2.37657
$\alpha = 30^\circ$	1.44169	0.00000	2.55844
$\alpha = 45^\circ$	1.42970	0.00000	2.59826
$\alpha = 60^\circ$	1.53821	0.18744	2.70667
$\alpha = 90^\circ$	1.76844	2.91317	1.89907

Table 5
Effects of enclosure inclination angle on the average Nusselt and the absolute maximum and minimum stream function values for $\mathrm{Ha} = 70$, $\mathrm{Pr} = 0.025$, and $\mathrm{Ra} = 10^6$.

Parameter	$\overline{\mathrm{Nu}}$	$\lvert\psi_{\max}\rvert$	$\lvert\psi_{\min}\rvert$
$\alpha = 0^\circ$	4.17966	0.00000	11.28673
$\alpha = 30^\circ$	4.55997	0.00000	13.09854
$\alpha = 45^\circ$	4.51586	0.00000	13.45652
$\alpha = 60^\circ$	4.30850	0.00000	13.31289
$\alpha = 90^\circ$	5.99377	14.41331	13.66526

Table 6
Effects of enclosure inclination angle on the average Nusselt and the absolute maximum and minimum stream function values for $\mathrm{Ha} = 70$, $\mathrm{Pr} = 0.007$, and $\mathrm{Ra} = 10^5$.

Parameter	$\overline{\mathrm{Nu}}$	$\lvert\psi_{\max}\rvert$	$\lvert\psi_{\min}\rvert$
$\alpha = 0^\circ$	1.38115	0.00000	2.50879
$\alpha = 30^\circ$	1.40115	0.00000	2.50985
$\alpha = 45^\circ$	1.35212	0.00000	2.26916
$\alpha = 60^\circ$	1.28838	0.00000	2.06330
$\alpha = 90^\circ$	1.53675	2.51769	1.54203

that the values of $\overline{\mathrm{Nu}}$ and $|\psi_{\min}|$ decrease while the values of $|\psi_{\max}|$ increase as Pr decreases for all values of α. In addition, the same non-monotonic variation in the values of $\overline{\mathrm{Nu}}$ as those discussed in Table 5 is predicted. Also, the values of $|\psi_{\max}|$ are predicted to remain unchanged at the value of zero for angles between $\alpha = 0^\circ$ and $\alpha = 60^\circ$ and they increase for the case where $\alpha = 90^\circ$ while the values of $|\psi_{\min}|$ reach a slight maximum for $\alpha = 30^\circ$ and then decrease for higher enclosure inclination angles.

Conclusions

Natural convective flow of electrically-conducting gallium or germanium liquid metals in an inclined rectangular enclosure in the presence of a uniform magnetic field due to a transverse temperature gradient was studied numerically. The governing equations for this investigation were put in the dimensionless vorticity – stream function formulation and were solved by the finite-difference method. Graphical results for the streamline and temperature contours and representative velocity and temperature profiles at the enclosure mid-section for various parametric conditions were presented and discussed. It was found that in the absence of a magnetic field a three-cellular structure exits. However, this behavior does not exist for relatively weak magnetic fields where a single-cell structure dominates. On the other hand, for a relatively strong magnetic field, mutiple-cellular streamline structure is predicted for enclosure inclination angles between 45° and 90°. Also, it was predicted that the heat transfer and the flow characteristics inside the enclosure depended strongly on the strength of the magnetic field, the enclosure inclination or tilting angle and the Rayleigh number. The presence of the magnetic field was found to reduce the average Nusselt number significantly. In addition, it was predicted that the values of the average Nusselt number varied non-monotonically with increasing enclosure inclination angles. The exact inclination angle for which the average Nusselt number increases or decreases depended on the values of the fluid Prandtl and Rayleigh numbers for the fixed value of Hartmann number considered. It is hoped that the results obtained in the present work be compared at a later stage with those from a fully three-dimensional simulation in order to ascertain the actual influence of the neglected terms and the two-dimensionality assumption.

REFERENCES

1. Markham, B. L. and Rosenberger, F., Diffusive-Convective Vapor Transport across Horizontal and Inclined Rectangular Enclosures, *J. Cryst. Growth*, 1984, **67**, pp. 241–254.
2. Bontoux, P., Smutek, C., Randriamampianina, A., Roux, B., Extremet, G. P., Hurford, A. C., Rosenberger, F., and De Vahl, D., Numerical Solutions and Experimental Results for Three-Dimensional Buoyancy Driven Flows in Tilted Cylinders, In: *Adv. Space Resch*, New York, Pergamon, 1986, pp. 155–160.
3. Delgado-Buscalioni, R. and Crespo del Arco, E., Flow nd Heat Transfer Regimes in Inclined Differentially Heated Cavities, *Int. J. Heat Mass Transfer*, 2001, **44**, pp. 1947–1962.
4. Lock, G. S. H. and Fu, J., Natural Convection in the Inclined Cranked Thermosyphon, *J. Heat Transfer*, 1993, **115**, pp. 167–172.
5. Wirtz, R. A. and Tsheng, W. F., Natural Convection across Tilted Rectangular Enclosures of Small Aspect Ratio, *Natural Convection in Enclosures*, 1980, **8**, pp. 54–67.
6. Wirtz, R. A. and Tsheng, W. F., Finite Difference Simulation of Free Convection in Tilted Enclosures of Low Aspect Ratio, In: *Numerical Methods in Thermal Problems I*, Pineridge, UK, Swansea, 1970, pp. 381–390.

7. Woods, A. W. and Lintz, S. J., Natural Convection and Dispersion in Inclined Fracture, *J. Fluid Mech.*, **241**, 1992, pp. 59–74.
8. Cessi, P. and Young, W. R., Fixed-Flux Convection in a Tilted Slot, *J. Fluid Mech.*, 1992, **237**, pp. 57–71.
9. Cerisier, P. and Rahal, S., Experimental Study of the Competition between Convective Rolls in an Enclosure, In: *Dynamics of Multiphase Flows across Interfaces*, Pergamon, Oxford, 1995, pp. 105.
10. Di Piazzo, I. and Ciofalo, M., MHD Free Convection in a Liquid-Metal Filled Cubic Enclosure. I. Differential Heating, *Int. J. Heat Mass Transfer*, 2002, **45**, pp. 1477–1492.
11. Oreper, G. M. and Szekely, J., The Effect of an Externally Imposed Magnetic Field on Buoyancy Driven Flow in a Rectangular Cavity, *J. Crystal Growth*, 1983, **64**, pp. 505–515.
12. Ozoe, H. and Maruo, M., Magnetic and Gravitational Natural Convection of Melted Silicon Two-Dimensional Numerical Computations for the Rate of Heat Transfer, *JSME*, 1987, **30**, pp. 774–84.
13. Garandet, J. P., Alboussiere, T., and Moreau, R., Buoyancy Driven Convection in a Rectangular Enclosure with a Transverse Magnetic Field, *Int. J. Heat Mass Transfer*, 1992, **35**, pp. 741–748.
14. Alchaar, S., Vasseur, P., and Bilgen, E., Natural Convection Heat Transfer in a Rectangular Enclosure with a Transverse Magnetic Field, *ASME J. Heat Transfer*, 1995, **117**, pp. 668–673.
15. Buhler, L., Magnetohydrodynamic Flows in Arbitrary Geometries in Strong, Nonuniform Magnetic Fields – a Numerical Code for the Design of Fusion Reactor Blankets, *Fusion Technol.*, 1994, **27**, pp. 3–24.
16. Viskanta, R., Kim, D. M., and Gau, C., Three-Dimensional Natural Convection Heat Transfer of a Liquid Metal in a Cavity, *Int. J. Heat Mass Transfer*, 1986, **29**, pp. 475–485.
17. Tagawa, T. and Ozoe, H., Enhancement of Heat Transfer Rate by Application of a Static Magnetic Field during Natural Convection of a Liquid Metal in a Cube, *ASME J. Heat Transfer*, 1997, **119**, pp. 265–271.
18. Tagawa, T. and Ozoe, H., Enhanced Heat Transfer Rate Measured for Natural Convection in Liquid Gallium in a Cubical Enclosure under a Static Magnetic Field, *ASME J. Heat Transfer*, 1998, **120**, pp. 1027–1032.
19. Di Piazzo, I. and Ciofalo, M., MHD Free Convection in a Liquid-Metal Filled Cubic Enclosure. II. Internal Heating, *Int. J. Heat Mass Transfer*, 2002, **45**, pp. 1493–1511.
20. Rudraiah, N., Barron, R. M., Venkatachalappa, M., and Subbaraya, C. K., Effect of a Magnetic Field on Free Convection in a Rectangular Enclosure, *Int. J. Engng Sci.*, 1995, **33**, pp. 1075–1084.
21. Al-Najem, N., Khanafer, K., and El-Refaee, M., Numerical Study of Laminar Natural Convection in Tilted Enclosure with Transverse Magnetic Field, *Int. J. Numer. Meth. Heat Fluid Flow*, 1998, **8**, pp. 651–672.
22. Cramer, K. R. and Pai, S. I., *Magnetofluid Dynamics for Engineers and Applied Physicists*, Scripta Publishing Company, Washington, DC, 1973.
23. Müller, G., *Convection and Inhomogeneities in Crystal Growth from the Melt*, Springer-Verlag, Berlin/Heidelberg, 1988.

□◆◆◆□